Peer-reviewed version available at Metals 2018, 8, 193; doi:10.3390/met8030193

Article

Evaluation of Workability on Microstructure and Mechanical Property of Modified 9Cr-2W Steel for Fuel Cladding by Cold Drawing Process and Intermediate Heat Treatment Condition

Hyeong-Min Heo [1], Jun-Hwhan Kim [2], Sung-Ho Kim [2], Jong-Ryoul Kim [1,*]

[1] Department of Materials Engineering, Hanyang University, 55, Hanyangdaehak-ro, Sangnok-gu, Ansan-si, Republic of Korea

[2] Advanced Fuel Development Division, KAERI, 989-111 Daedeok-daero, Yuseong-gu, Daejeon, 305-353, Republic of Korea

* **Correspondence: jina@hanyang.ac.kr; Tel.:+82-31-400-4279**

Abstract: In this study, we evaluated the cold drawing workability of two kinds of modified 9Cr-2W steel containing different contents of boron and nitrogen, depending on the temperature and time of normalizing and tempering treatments. Using ring compression tests at room temperature, the effect of intermediate heat treatment condition on workability was investigated. It was found that the prior austenite grain size can be changed by the austenite transformation, and the grain size increases with increasing temperature during normalizing heat treatment. Alloy B and Alloy N showed different patterns after normalizing heat treatment. Alloy N had higher stress than Alloy B, and the reduction in alloy N increased, while the reduction in alloy B decreased. Alloy B showed a larger number of initially formed cracks and a larger average crack length than Alloy N. Crack length and number increased proportionally in Alloy B as the stress increased. Alloy B had lower crack resistance than Alloy N due to boron segregation.

Keywords: intermediate heat treatment; boron; fabrication process

1. Introduction

A Generation IV SFR (sodium-cooled fast reactor) uses liquid sodium as a coolant and creates nuclear fission using fast neutrons [1]. The main components of the SFR are the nuclear fuel assemblies and nuclear fuel cladding. Because irradiation with fast neutrons generates thermal creep and swelling, the nuclear fuel cladding tube needs to provide excellent swelling resistance, creep resistance and high temperature strength for long periods of time. To meet these requirements, the nuclear fuel cladding of sodium cooled fast reactors is typically 9-12% FM (ferritic martensitic) steel, which exhibits outstanding thermal conductivity, a low thermal expansion coefficient, and high resistance to void swelling [2].

Nonetheless, 9-12% Cr FM steels have a problem, because their high temperature strength and creep characteristics deteriorate when they are subjected to high temperature for long periods of time. To improve mechanical properties such as creep strength and high temperature strength, the steel's carbon content can be optimized by the addition of Mo and W, which are solid solution hardening elements, and Nb and V, which are elements that form carbides and nitrides [3]. Boron is also known to reduce the coarsening of $M_{23}C_6$ carbides and decrease minimum creep rate, which improves microstructure stability and improves the creep life of the material [4]. Nitrogen reacts to precipitation hardening elements such as V, Nb, Cr to form fine nitrides (Nb, V)N and Cr_2N. These nitrides effectively contribute to the high-temperature creep properties, and improve microstructure stability, due to their extremely high thermal stability [5].

Peer-reviewed version available at Metals 2018, 8, 193; doi:10.3390/met8030193

In previous studies, nuclear fuel cladding has been fabricated using several procedures. These include VIM (vacuum induction melting), hot working such as hot forging and hot extrusion, and cold working such as cold pilgering, which reduces the thickness and outer diameter by more than 90%, and several cold drawing methods with intermediate heat treatment. After fabrication with the desired specifications the manufactured nuclear fuel cladding tube is finally normalized and tempered. Some studies have shown that when boron and nitrogen are added to improve creep characteristics and mechanical properties, the additives also affect the material's workability, depending on content and heat treatment [6,7].

9-12% Cr FM steel was used to conduct a SIMS analysis of the distribution of boron at grain boundaries caused by the effects of normalizing and tempering [8]. Studies on high temperature ductility were carried out to examine surface cracks and corner cracks which occur during the continuous casting process in boron added steel [9]. Boron has been reported to change its mechanical properties depending on the cooling rate, the heat treatment temperature [10]. These indicate that boron precipitates as compounds such as BN and $M_{23}(B, C)_6$ at grain boundaries, weakening the grain boundary and reducing high temperature ductility [11].

In this study, we evaluated the cold drawing workability of two kinds of modified 9Cr-2W steel with different contents of boron and nitrogen, depending on normalizing and tempering temperature and time. Ring compression testing at room temperature was used to investigate the effect of heat treatment on workability.

2. Materials and Methods

The chemical compositions of the two different kinds of modified 9Cr-2W steel, designated Alloy B and Alloy N, are shown in Table 1.

Table 1 Chemical compositions of the modified 9Cr-2W steels (wt %).

	C	Cr	W	N	B	Fe
Alloy B	0.07	8.89	1.934	0.02	0.013	Bal.
Alloy N	0.063	9.09	2.019	0.0767	0.004	Bal.

The modified 9Cr-2W steel ingot was melted in VIM (vacuum induction melting) and then hot-forged at 1170°C to form rods. The fabricated modified 9Cr-2W steel rods were processed into billets and hot extruded at 1170°C to produce extruded pipes with a 46 mm outer diameter and 3.5 mm thickness. The manufactured mother tube was finally fabricated into a drawn tube with a 19.05 mm outer diameter and 1.15 mm thickness by a cold drawing process.

The drawn tubes were sealed in quartz tubes in an atmosphere of argon gas, and then normalized at 1038-1180°C for 6 and 30 min, followed by air cooling to room temperature. A tempering treatment of the normalized specimens was carried out at 760°C for 40 min, followed by air cooling to room temperature. The heat treatment conditions of the modified 9Cr-2W steel are shown in Table 2. In order to observe the microstructure produced by the particular heat treatment condition, the specimens were observed by optical microscope after etching with a mixed solution of HF (hydrofluoric acid): HNO_3 (nitric acid): H_2O (distilled water) = 2: 3: 95.

Preprints (www.preprints.org) | NOT PEER-REVIEWED | Posted: 8 January 2018 doi:10.20944/preprints201801.0056.v1

Peer-reviewed version available at Metals 2018, 8, 193; doi:10.3390/met8030193

Table 2 Heat treatment conditions of the modified 9Cr-2W steels.

	Normalizing	Tempering
Alloy B	1038°C, 6min 1038°C, 30min	760°C, 40min
AlloyN	1100°C, 6min 1180°C, 6min	
	X	760°C, 40min

In order to evaluate the mechanical properties and workability of the Modified 9Cr-2W steel as a result of the particular heat treatment conditions, ring compression testing was performed at room temperature using an INSTRON-3367.

The cold pilgering and cold drawing induce tensile stress in the axial direction, and compressive stress in the circumferential direction. Ring compression tests have also been conducted to evaluate the workability of zirconium alloys after cold pilgering [12]. In this test, compressive stress after cold working was evaluated. The compression test specimens were compressed at a rate of 1 mm/min for cladding with a 19.05 mm outer diameter and 1.15 mm thickness and 10 mm length. We performed ring compression tests at room temperature based on the heat treatment conditions, and used a stereoscope to observe the shape of cracks produced by the respective heat treatment conditions.

In order to investigate the change in hardness produced by the various heat treatment conditions, the Vickers hardness test was performed. The results were measured 12 times for each specimen under a load of 500g, and the minimum and maximum values were excluded, and then standard deviation and mean were evaluated.

3. Results

3.1. Changes in microstructure according to heat treatment conditions

Figure 1 and 2 show photographs of Alloy B and Alloy N following heat treatment, respectively. The pilgering and drawing processes created an elongated grain boundary in the drawing direction in the as-drawn specimens.

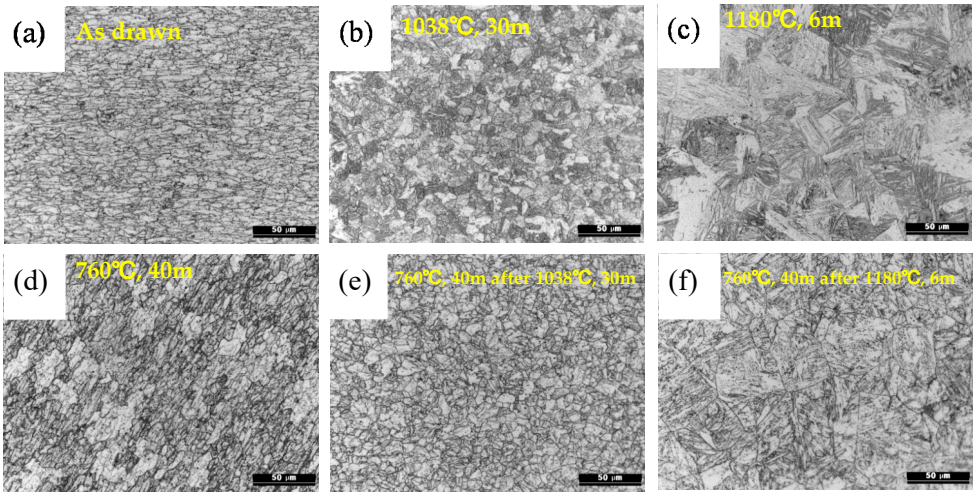

Figure 1 Optical micrographs of Alloy B for different heat treatment conditions: (a) as-drawn, (b) normalized at 1038℃ for 30 min, (c) normalized at 1180℃ for 6 min, (d) tempered at 760℃ for 40 min after as-drawn, (e) tempered at 760 for 40 min after normalized at 1038℃ for 30min and (f) tempered at 760 for 40 min after normalized at 1180℃ for 6min

On the other hand, elongated grain boundary disappears in the normalized condition. (d) indicates the tempering heat condition, after a treatment at 760°C for 40 minutes without a normalizing heat treatment.

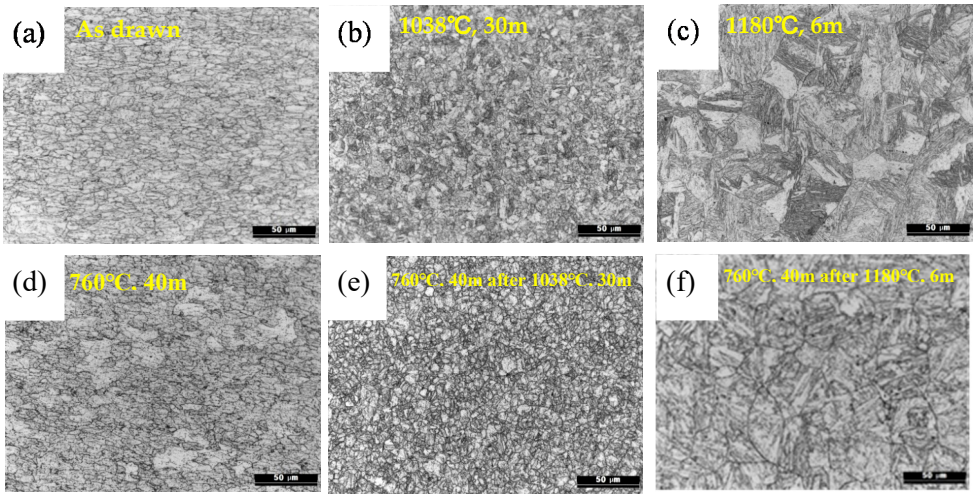

Figure 2 Optical micrographs of Alloy N for different heat treatment conditions: (a) as-drawn, (b) normalized at 1038℃ for 30 min, (c) normalized at 1180℃ for 6 min, (d) tempered at 760℃ for 40 min after as-drawn, (e) tempered at 760 for 40 min after normalized at 1038℃ for 30min and (f) tempered at 760 for 40 min after normalized at 1180℃ for 6min

Figure 3 shows the effect on austenite grain size for Alloy B and Alloy N, based on normalizing conditions. In the initial state as-drawn Alloy B and Alloy N have an austenite grain size of 48 and 55 μm, respectively. In particular, at 1180°C the prior austenite grain size increased to more than twice the size of the prior austenite grain at 1038°C.

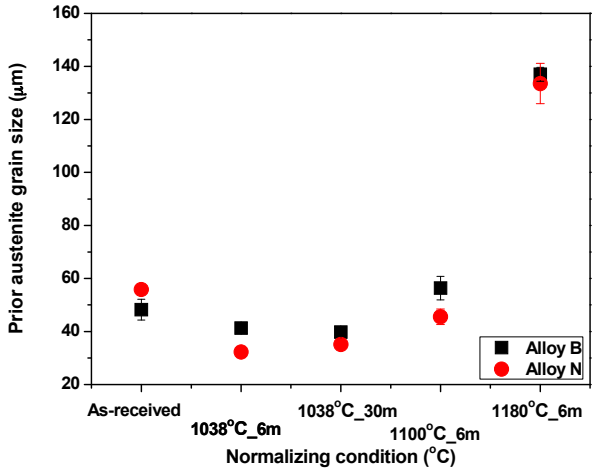

Figure 3 Variation in prior austenite grain size of Alloy B and Alloy N with different normalizing conditions

3. 2 Effect of heat treatment conditions on mechanical properties

Figure 4 shows a specimen (Alloy B) normalized at 1038°C for 6 min. A ring compression test was conducted at room temperature and the results are represented in the schematic diagram. The ring compression test was performed by pressing the sample in the cladding tube with a plate fixed top and bottom, at a constant strain rate. The cladding tube gradually turns into an ellipse, because the applied stress deforms the cladding tube as the axial load on the cladding tube increases. The

Preprints (www.preprints.org) | NOT PEER-REVIEWED | Posted: 8 January 2018 doi:10.20944/preprints201801.0056.v1

Peer-reviewed version available at Metals 2018, 8, 193; doi:10.3390/met8030193

aspects of the cracks at maximum compressive stress were found to be different for the normalizing condition, as compared to the tempering condition. In the normalizing condition, the generated cracks grew and then failed due to interactions, as the stress was increased.

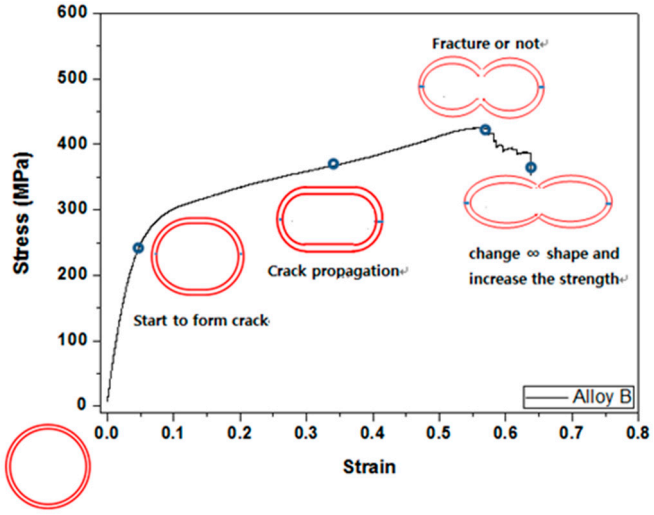

Figure 4 Stage of ring compression test (1038°C, 6m)

However, with the tempering condition, many cracks tended to occur, but unlike the normalizing condition case, when the stress increased, the length and width of the cracks increased, but the cracks did not interact with cracks grew and then failed due to interactions, as the stress was increased.

Figure 5 shows the results of maximum compressive strength and stiffness for the ring compression testing at room temperature, based on heat treatment conditions. The results for the as-drawn steels show that the maximum compressive stress of alloy B is higher than that of alloy N. Since the prior austenite grain size of alloy N is larger than that of alloy B, the maximum compressive stress of alloy N has a smaller value in the Hall-Petch equation. The stress in alloy N has a higher value than that of alloy B after normalizing.

(a)

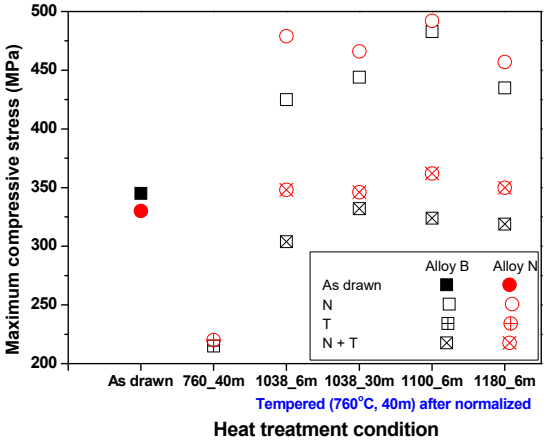

Preprints (www.preprints.org) | NOT PEER-REVIEWED | Posted: 8 January 2018 doi:10.20944/preprints201801.0056.v1

Peer-reviewed version available at Metals 2018, 8, 193; doi:10.3390/met8030193

(b)

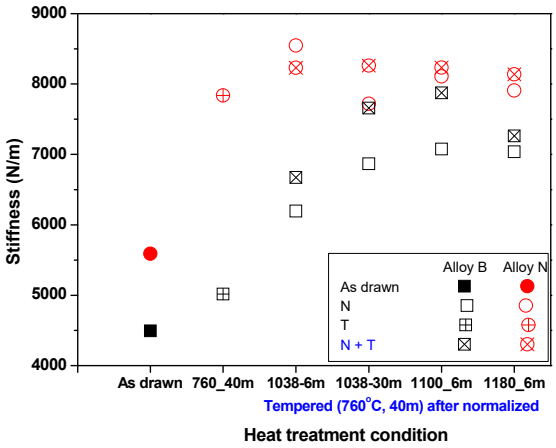

(c)

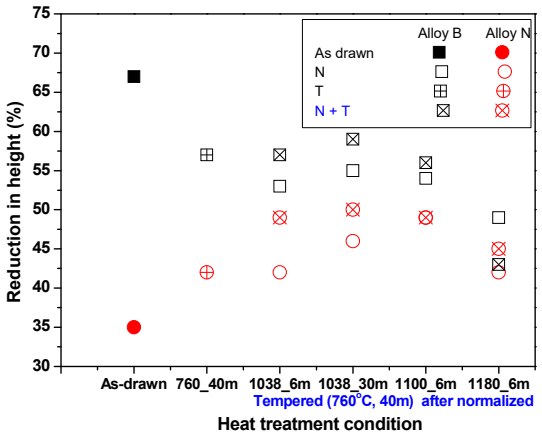

Figure 5 Results of ring compression test with heat treatment condition for Alloy B and Alloy N: (a) Maximum compressive stress, (b) stiffness and (c) reduction in height

Both alloys were normalized by heat treatment, and below 1100°C the prior austenite grain size was less than that of the as-drawn samples. The prior austenite grain sizes increased but higher than the stress of the as-drawn samples after heat treatment above 1100°C.

Overall, the stiffness of Alloy N was found to be higher than that of Alloy B, and Alloy N had a constant stiffness after heat treatment. On the other hand, Alloy B exhibited a higher stiffness than that of as-drawn B when it was annealed at 760°C for 40 min.

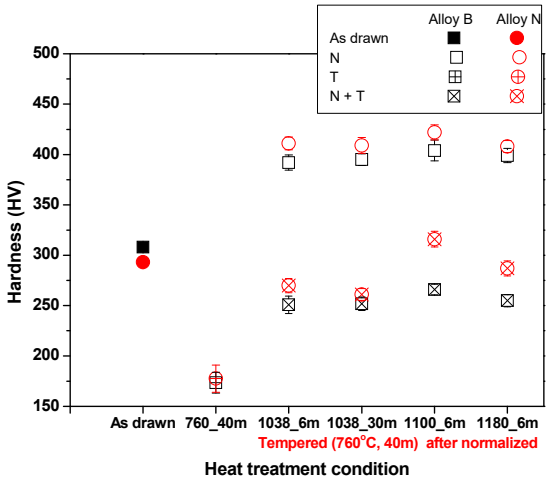

Figure 6 Results of hardness testing with heat treatment condition for Alloy B and Alloy N

Normalized specimens of the two alloys were tempered at 760°C for 40 min and had high stiffness. Therefore, Alloy N was determined to have high resistance to deformation in response to an applied force.

Comparing the reduction in height of the two alloys, the reduction in height of as-drawn B was higher than that of as-drawn N. The reduction in height of the two alloys was different before and after the normalizing heat treatment. In the case of Alloy B, the reduction in height decreased as the normalizing temperature increased.

Figure 6 shows the hardness results based on heat treatment. These results show a tendency similar to that for stress.

3. 3 Crack formation and observation

Figure 7 shows photographs of cracks and the number and length of cracks for the as-drawn conditions. The crack lengths and the numbers of cracks were compared in order to determine the effect on workability induced by crack resistance during fuel cladding manufacture. Cracks were formed in the Alloy B when stress reached 241MPa, while in alloy N cracks were generated when stress reached 310MPa.

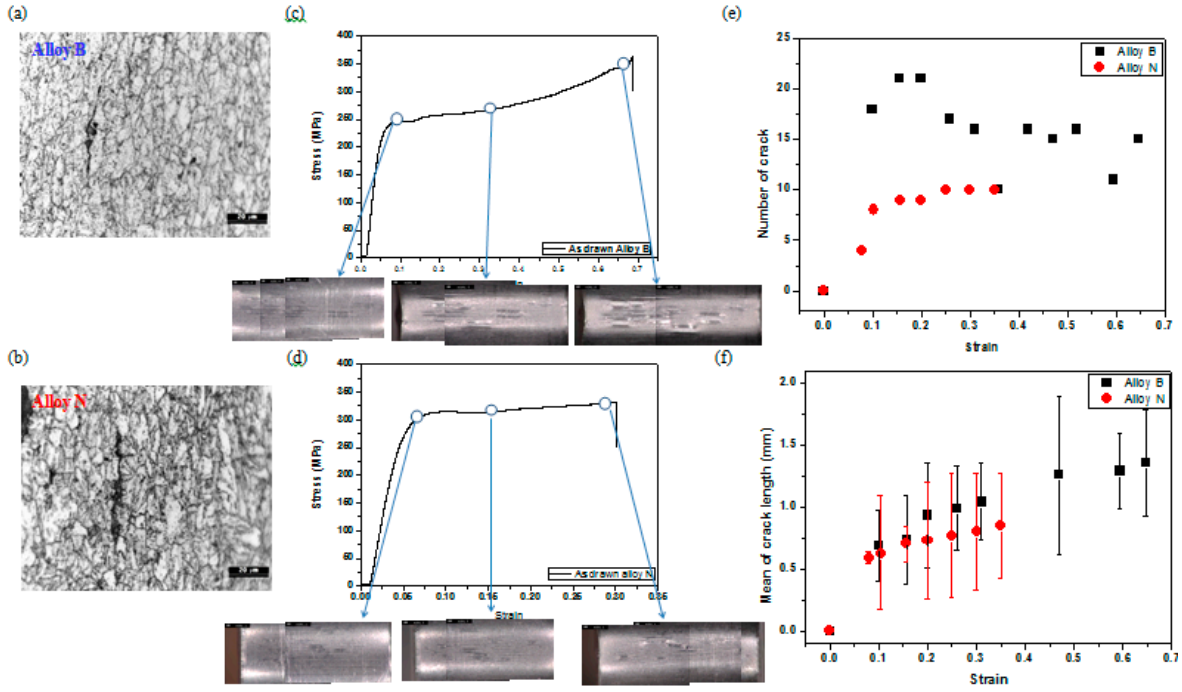

Figure 7 Observation of cracks by OM image (a-b), Stress-strain curve and stereo image (c-d), (e) number of cracks depending on strain and (d) mean of crack length depending on strain

Figure 8 shows cracks that were observed after carrying out compression testing at room temperature, based on heat treatment conditions. Between temperatures of 1038 to 1100°C, multiple cracks were generated when the maximum compressive stress was reached, and when the maximum tensile stress was applied in the longitudinal direction, the existing cracks were connected and formed into a shape like stair steps. As the tensile stress increased in the axial direction in the center part in the specimen at 1180°C, the sample seemed to be fractured by an existing single crack. Multiple cracks existed without connecting in the tempering condition. The tempering heat treatment changed the sample from a martensitic structure with brittleness to a tempered martensitic structure with increasing ductility, and following the transition the cracks were different in appearance.

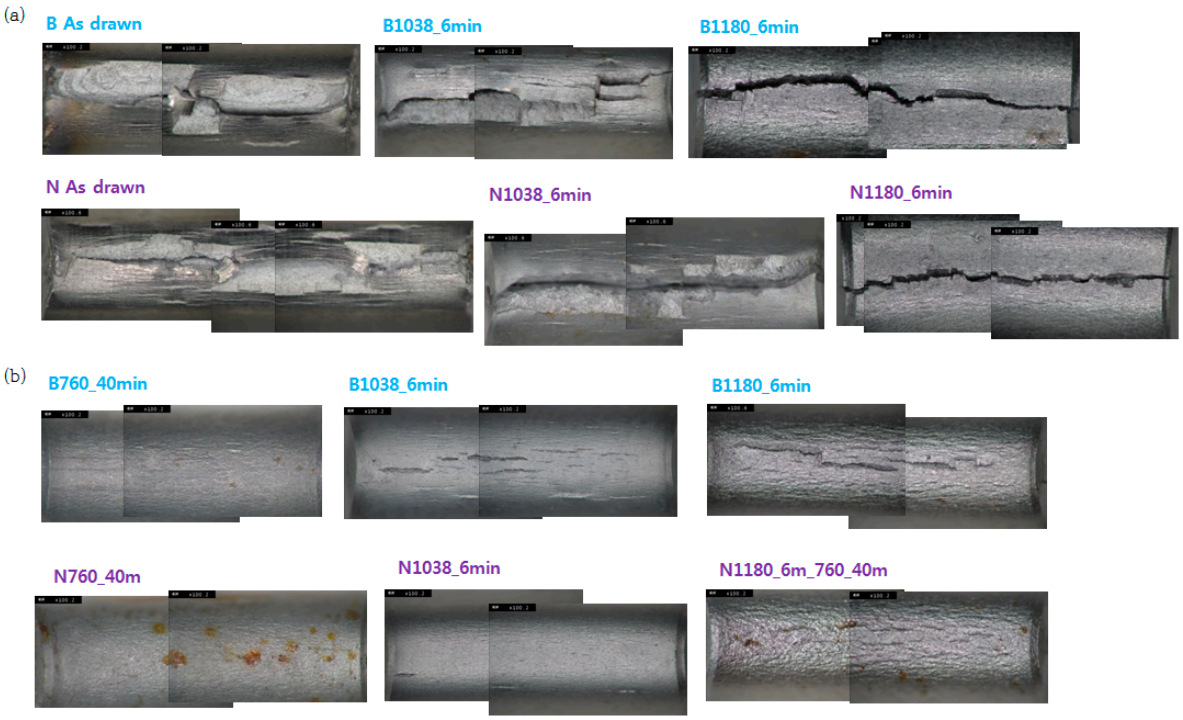

Figure 8 Observation of cracking with heat treatment (a) normalizing condition and (b) tempering condition (760℃, 40 min after normalizing)

4. Discussion

This study investigated the mechanical properties of cladding tubes fabricated with two types of alloy, Alloy B and Alloy N, and evaluated the effects of normalizing and tempering heat treatments on the workability of the tubes, which is required for manufacturing cladding tube. In Figure 1 and 2, as drawn specimen has an elongated grain boundary in the drawing direction due to deformation by drawing and pilgering process. On the other hand, the deformed microstructure was transformed into an austenitic structure by heating at the AC_3 transformation point or higher in the normalized condition. The deformed structure disappears due to recrystallization, and forms a lath martensitic structure with a high dislocation density after air cooling [13]. The tempering heat treatment does not cause recrystallization, so some deformed microstructure remains. A typical tempered martensitic structure is produced by the tempering condition after normalizing. There is no recrystallization during the tempering heat treatment, and the strength decreases and the ductility increases due to dislocation recovery, but the previous austenite grain size is not affected [14].

The change of prior austenite grain boundary size is related to normalizing temperature. When the as-drawn specimens were normalized at 1038°C, the austenite transformation resulted in recrystallization of the deformed microstructure and an increase in nucleation sites, resulting in smaller grain sizes. At a normalizing temperature above 1100°C, the grain sizes increased because the growth rate of the grain was faster than the rate at which the nucleation sites occurred. As the normalizing temperature increases, compressive stress also increases. During the normalizing heat treatment, carbide is solubilized in the matrix and has a low fraction of precipitate, which increases the stress induced by carbon in the matrix[14]. When the as-drawn conditions were tempered at 760°C for 40 min, stress was reduced because the dislocation density decreased, and solute atoms in the matrix precipitated with a high fraction precipitate [14].

Stiffness is the rigidity of an object against deformation in response to an applied force. This resistance is a property of the structure or a component of the structure, and hence it is dependent

Peer-reviewed version available at Metals 2018, 8, 193; doi:10.3390/met8030193

upon the various physical dimensions which describe that component. For example, for an element in tension or compression, the axial stiffness is

$$k = \frac{AE}{L}$$

where A is the cross section area, E is the (tensile or compression) elastic modulus (or Young's modulus), and L is the length of the element.

Cracks are generated because the stress applied to the material changes elastic regions into plastic regions during ring compression test at room temperature. These are thought to be formed by the accumulation of many small cracks in a direction that is tangential to the inner surface. It appears that more than 10% tensile strain is sufficient to produce the occurrence of cracks [15]. The cracks are generated in the grain boundaries. The grain boundary between boron and steel is known to occur due to equilibrium and non-equilibrium segregation [16]. Equilibrium grain boundary segregation occurs with the movement of solute atoms from the matrix to grain boundaries and free surfaces. The driving force for the equilibrium segregation is the reduction in the grain boundary free energy. NGS (Non-equilibrium grain boundary segregation) occurs during cooling from high temperatures when mobile vacancy-solute complexes diffuse down vacancy gradients towards vacancy sinks [16]. The NGS mechanism depends on the formation of sufficient quantities of vacancy-solute complexes. It has been widely accepted that the NGS of boron in steel is the dominating process [17].

Since the vacancy concentration also increases as the normalizing temperature increases, the vacancy-solute complexes increase and the segregation of boron often occurs at the grain boundary. Segregation of boron may weaken the grain boundary bonding force. Therefore, the reduction in height is decreased by the segregation of boron, and it decreases especially sharply at 1180°C. In the case of Alloy N, the reduction in height increased as the normalizing temperature increased. During the normalizing heat treatment, carbide is solubilized in the matrix and has a low fraction of precipitate, which decreases the interaction between carbon and dislocations. As a consequence, the reduction in height increases as the normalizing temperature increases.

When as-drawn Alloy B samples were tempered at 760°C for 40 min, the decrease in height reduction was attributed to the segregation of boron. Some studies have analyzed the tempering heat treatment by APT (atom probe tomography). The APT results show that the concentrations of Cr, Mo, V and Mn in the matrix decrease, and then Nb, B and N are depleted from the matrix. It is noteworthy that the $M_{23}C_6$ precipitate at a PAGB contains a very high concentration of boron [8]. Segregation were analyzed from the view point of grain boundary characteristics by using EBSD (Electron back scattered diffraction) [18]. It is well known that the segregation is thermodynamically preferential to occur at high energy boundaries such as high angle random boundaries (Prior austenite grain boundary and packet boundary) [19].

Comparing the two alloys, a larger number of cracks initially formed in Alloy B, and the cracks had a larger average length than those in Alloy N. The cracks in Alloy B increased proportionally as the stress increased. Alloy B had a lower crack resistance than Alloy N. The reason for the low crack resistance of Alloy B is considered to be weakening of grain boundary due to segregation of excess boron.

5. Conclusion

This study investigated the mechanical properties of cladding tubes fabricated with two types of alloy, Alloy B and Alloy N, and evaluated the effects of normalizing and tempering heat treatments on the workability of the tubes, which is required for manufacturing cladding tube. The difference in stress of the as-drawn alloys was indicated by the difference in prior austenite grain size. The prior austenite grain size can be changed by the austenite transformation, and the grain size was found to increase with increasing normalizing temperature in the normalizing heat treatment process. The stiffness of Alloy N was determined to be higher than that of Alloy B, and Alloy N had a constant

stiffness after heat treatment. On the other hand, Alloy B had a higher stiffness than that of as-drawn B when it was annealed at 760°C for 40 minutes.

Normalized specimens of the two alloys were tempered at 760°C for 40 minutes, and exhibited high stiffness. Alloy N was determined to have high resistance to deformation in response to an applied force. Cracks were formed in Alloy B when applied stress reached 241MPa, while cracks in Alloy N were generated when stress reached 310MPa. Comparing the two alloys, Alloy B showed a larger number of initially formed cracks and a larger average crack length, than Alloy N. Cracking in Alloy B increased proportionally as the stress increased, and Alloy B had a lower crack resistance than Alloy N. The reason for the low crack resistance of Alloy B is considered to be weakening of grain boundary due to segregation of excess boron.

After tempering treatment, multiple cracks existed, but without connecting. The tempering heat treatment changes the steel from a martensitic structure with brittleness to a tempered martensitic structure with increasing ductility, and following the change the cracks are different in appearance.

Acknowledgments: This work was done by the 'SFR Cladding Development Project' supported by the National Nuclear R&D program through the Sodium-cooled Fast Reactor development Agency funded by Ministry of Science, Ict & Future Planning.

Author Contributions: J. H. Kim designed the experiments; J. R. Kim contributed to the discussion of the results; H. M. Heo performed the experiments and wrote the paper; S. H. Kim Supervised the project.

Conflicts of Interest: The authors declare no conflict of interest.

References

1. Kim, J. H.; Heo, H. M.; Baek, J. H.; Kim, S. H. Evaluation of the mechanical properties of a HT9 fuel cladding tube for a sodium-cooled fast reactor. *J. Korean Inst. Met. Mater.* **2013**, *51*, 25–31, doi:10.3365/KJMM.2013.51.1.025.
2. Klueh, R. L. Elevated-Temperature Ferritic and Martensitic Steels and Their Application To Future. *Int. Mater. Rev.* **2005**, *50*, 287–310.
3. Thomas Paul, V.; Saroja, S.; Vijayalakshmi, M. Microstructural stability of modified 9Cr-1Mo steel during long term exposures at elevated temperatures. *J. Nucl. Mater.* **2008**, *378*, 273–281, doi:10.1016/j.jnucmat.2008.06.033.
4. Abe, F. Effect of Boron on Microstructure and Creep Strength ofAdvanced Ferritic Power Plant Steels. *Procedia Eng.* **2011**, *10*, 94–99, doi:10.1016/j.proeng.2011.04.018.
5. Ryu, W. S.; Kim, S. H. Thermal treatment improving creep properties of nitrogen-added Mod . 9Cr-1Mo steels. *Trans. Indian Institue Met.* **2010**, *63*, 111–115.
6. Lu, Y. Effect of Boron on Microstructure and Mechanical Properties ofLow Carbon Microalloyed Steels, McGil University, 2007.
7. Kim, Y. H.; Kim, K. Y.; Lee, Y. D. Nitrogen-Alloyed, Metastable Austenitic Stainless Steel for Automotive Structural Applications. *Mater. Manuf. Process.* **2004**, *19*, 51–59, doi:10.1081/AMP-120027498.

8. Liu, F.; Fors, D. H. R.; Golpayegani, A.; Andrén, H. O.; Wahnström, G. Effect of boron on carbide coarsening at 873 K in 9 to 12 pct chromium steels. *Metall. Mater. Trans. A Phys. Metall. Mater. Sci.* **2012**, *43*, 4053–4062, doi:10.1007/s11661-012-1205-6.
9. Cho, K.; Koo, Y.; Park, J. Effect of cooling rate on the hot ductility of boron bearing steel during continuous casting (Study for prevention of corner crack on continuous casting slab). *J. Kor. Inst. Met. Mater.* **2008**, *46*, 329–337.
10. Lim, J.; Kim, J.; Park, B.; Lee, J.; Choi, J. Effects of Heat Treatment on the Micro-structures and the Mechanical Properties of 0.002% Boron-added Low Carbon Steel. *Kor. J. Mater. Res.* **2011**, *21*, 303–308, doi:10.3740/MRSK.2011.21.6.303.
11. Yamamoto, K.; Susuki, H. G.; Oono, Y.; Noda, N.; Inoue, T. Formation mechanism and prevention method of facial cracks of continuously cast steel slabs containing boron. *Tetsu-to-Hagane* **1987**, *73*, 115–122.
12. Abe, H.; Furugen, M. Evaluation Method of Workability in Cold Pilgering of Zirconium-based Alloy Tube. *Mater. Trans.* **2010**, *51*, 1200–1205, doi:10.2320/matertrans.P-M2010812.
13. Saroja, S.; Vijayalakshmi, M.; V.S., R. Influence of cooling rates on the transformation behaviour of 9Cr-1 Mo-O.07C steel. *J. Mater. Sci.* **1992**, *27*, 2389–2396.
14. Barbadikar, D. R.; Deshmukh, G. S.; Maddi, L.; Laha, K.; Parameswaran, P.; Ballal, a. R.; Peshwe, D. R.; Paretkar, R. K.; Nandagopal, M.; Mathew, M. D. Effect of normalizing and tempering temperatures on microstructure and mechanical properties of P92 steel. *Int. J. Press. Vessel. Pip.* **2015**, *132–133*, 97–105, doi:10.1016/j.ijpvp.2015.07.001.
15. Yamada, R.; Suzuki, M.; Harayama, Y. Application of finite element method to ring compression test. *Nucl. Eng. Des.* **1977**, *44*, 75–85.
16. Mun, D. J.; Shin, E. J.; Koo, Y. M. A study on the behavior of boron distribution in low carbon steel by particle tracking autoradiography. *Nucl. Eng. Technol.* **2011**, *43*, 1–6, doi:10.5516/NET.2011.43.1.001.
17. Williams, T. M.; Stoneham, a. M.; Harries, D. R. The segregation of boron to grain boundaries in solution-treated Type 316 austenitic stainless steel. *Met. Sci.* **1976**, *10*, 14–19, doi:10.1179/030634576790431471.
18. Park, S.; Lee, K.; Kim, M.; Lee, B. Effects of boundary characteristics on resistance to temper embrittlement and segregation behavior of Ni – Cr – Mo low alloy steel. *Mater. Sci. Eng. A* **2013**, *561*, 277–284, doi:10.1016/j.msea.2012.10.078.
19. Militzer, M.; Wieting, J. Segregation mechanisms of temper embrittlement. *Acta Metall.* **1989**, *37*, 2585–2593, doi:10.1016/0001-6160(89)90292-7.